Patterns of Coordinated Anatomical Change in Human Cortical Development: A Longitudinal Neuroimaging Study of Maturational Coupling

Armin Raznahan,[1,*] Jason P. Lerch,[2,3] Nancy Lee,[1] Dede Greenstein,[1] Gregory L. Wallace,[1] Michael Stockman,[1] Liv Clasen,[1] Phillip W. Shaw,[1] and Jay N. Giedd[1]

[1]Child Psychiatry Branch, National Institute of Health, National Institutes of Mental Health, Bethesda, MD 20892, USA
[2]Neuroscience and Mental Health, The Hospital for Sick Children, Toronto, ON M5G 1X8, Canada
[3]Department of Medical Biophysics, University of Toronto, Toronto, ON M5G 2M9, Canada
*Correspondence: raznahana@mail.nih.gov
DOI 10.1016/j.neuron.2011.09.028

SUMMARY

Understanding of human structural brain development has rapidly advanced in recent years, but remains fundamentally "localizational" in nature. Here, we use 376 longitudinally acquired structural brain scans from 108 typically developing adolescents to conduct the first study of coordinated anatomical change within the developing cortex. Correlation in rates of anatomical change was regionally heterogeneous, with fronto-temporal association cortices showing the strongest and most widespread maturational coupling with other cortical areas, and lower-order sensory cortices showing the least. Canonical cortical systems with rich structural and functional interconnectivity showed significantly elevated maturational coupling. Evidence for sexually dimorphic maturational coupling was found within a frontopolar-centered prefrontal system involved in complex decision-making. By providing the first link between cortical connectivity and the coordination of cortical development, we reveal a hitherto unseen property of healthy brain maturation, which may represent a target for neurodevelopmental disease processes, and a substrate for sexually dimorphic behavior in adolescence.

INTRODUCTION

Longitudinal structural neuroimaging provides a powerful tool for developmental neuroscience because of its unique ability to measure anatomical change within the same individual over time. In recent years, studies using this approach have yielded fundamental insights into the dynamic nature of typical human brain maturation, and the ways in which neurodevelopment can differ according to sex, cognitive ability, genetic profile, and disease status (Giedd and Rapoport, 2010). To date, however, published studies of developmental changes in brain anatomy have considered each cortical location in statistical isolation from all others (although intriguing qualitative descriptions of coordinated anatomical change in the developing human brain have begun to emerge [Hill et al., 2010]). Resultantly, while it is now clear that changes in cortical anatomy en route to adulthood show marked regional heterogeneity in humans (Gogtay et al., 2004; Shaw et al., 2008; Sowell et al., 2004), the relationships between structural change in different parts of the developing cortical sheet remain unquantified. Similarly, while factors such as sex (Raznahan et al., 2010) and disease status (Vidal et al., 2006) have now been linked to focal differences in the rate of structural cortical maturation—the possibility that these factors could also modify how different cortical regions change in relation to one another remains unexamined. A primary obstacle to studying the coordination of cortical development in humans has been the slow pace with which detectable maturational changes in cortical anatomy unfold (Shaw et al., 2008). Consequently, there are very few longitudinal neuroimaging studies of sufficient size and longevity to permit correlational analysis of developmental changes in cortical structure.

Here, we use the largest and longest-running longitudinal neuroimaging study of human brain maturation (Gordon et al., 1994; Raznahan et al., 2011) to describe and analyze in vivo patterns of correlated anatomical change within the cortex across the sensitive developmental window of late childhood, adolescence, and early adulthood (Paus et al., 2008). We included 108 typically developing individuals on whom a total of 376 structural magnetic resonance imaging (sMRI) brain scans, had been gathered between ages 9 and 22 years. Measures of cortical thickness (CT) were taken at ~82,000 points (vertices) on the cortical surface of each scan with submillimeter resolution (Lerch and Evans, 2005; MacDonald et al., 2000). At least three (and up to six) sMRI scans had been acquired on each participant at ~2 year intervals over the developmental period in question, These data allowed us to generate an estimate of annual CT change at each vertex, in each participant. This re-representation of repeat sMRI measures of brain anatomy as person-specific maps of anatomical change enabled us to interrelate the diverse maturational tempos that exist within the growing cortical sheet (Gogtay et al., 2004; Shaw et al., 2008) by asking how interindividual differences in rate of change at one cortical locus predicted those at another.

We focused on cortical thickness (CT) as our anatomical index of interest because; it can be validly and reliably (Kabani et al., 2001; Kim et al., 2005; Lerch and Evans, 2005; Shaw et al., 2008) mapped across the cortical sheet at high spatial resolution in a fully automated manner (MacDonald et al., 2000); its normative developmental trajectories during childhood, adolescence and early adulthood have been better described than those of any other morphometric aspect of the cortex (Raznahan et al., 2010; Shaw et al., 2008); and several studies have already examined cross-sectional CT correlations (He et al., 2007; Lerch et al., 2006; Sanabria-Diaz et al., 2010), thus providing a useful context within which to consider findings regarding correlated CT change.

Our first goal was to address the basic question of whether coordinated patterns of structural change can be identified in the developing cortex. The existence of such maturational coupling is suggested by evidence that cross-sectional measures of cortical anatomy show a highly organized correlational structure (He et al., 2007; Lerch et al., 2006; Sanabria-Diaz et al., 2010), and recognition that neurostructural variation at any one point in time is (at least in part) likely to reflect earlier variations in the rate of anatomical change. In order to discern patterns of correlated CT change within the brain, we adapted a methodology initially developed for studying cross-sectional CT correlations (Lerch et al., 2006), and used this to correlate the rate of CT change at each vertex with that at every other vertex on the cortical sheet. We predicted that patterns of correlated CT change would echo existing descriptions of cross-sectional CT correlation (Lerch et al., 2006), such that fronto-temporal cortices would show the strongest and most spatially extensive patterns of correlation with CT change in other cortical areas, while the maturational tempo of primary sensory cortices would be relatively uncoupled from that within the rest of the cortical sheet.

Next, we built on our description of correlated anatomical change by asking if maturational coupling within the cortex is structured according to known principles of brain organization. Specifically, we sought evidence in support of the hypothesis that cortical systems already established as showing strong and persistent structural and functional interconnectivity, would also show highly correlated rates of anatomical change. This hypothesis is prompted by experimental evidence of activity-dependent structural plasticity in the cerebral cortex from sMRI studies (Draganski et al., 2004; Hyde et al., 2009). These neuroimaging experiments imply that cortical regions sharing similar patterns of activation over the lifespan will develop under more similar sets of activity-related trophic influences than cortical regions that are functionally independent of each other. This notion is partly supported by evidence that cross-sectional patterns of functional and structural correlations within the human brain strongly echo each other (Seeley et al., 2009). In order to test for convergence between known patterns of functional and structural connectivity in the cortex, and patterns of coordinated cortical maturation, we used two complementary analytic approaches. First, we examined correlated rates of CT change within the cortical "default mode network" (DMN) (Raichle et al., 2001). The DMN provides an useful model for investigating the relevance of patterned neural activity for coor-

dinated brain maturation because it is a fundamental activational signature of the resting brain that exists across primates (Margulies et al., 2009; Vincent et al., 2007); discernible in humans during wakeful rest, sleep, and in the shift from introspective to goal-directed cognition (Buckner et al., 2008); established very early on in human development (Gao et al., 2009) with its core composition remaining largely (de Bie et al., 2011; Fair et al., 2008) stable across childhood and adulthood (Jolles et al., 2011; Supekar et al., 2010; Thomason et al., 2011); and highly invariable in its composition within and between individuals (Damoiseaux et al., 2006). The three core DMN nodes are well-established as lying within a medial posterior cortical region (mPC) that encompasses posterior cingulate and precuneus, the medial prefrontal cortex (mPFC), and lateral inferior parietal cortex (iPC) (Buckner et al., 2008). Of these, the mPC node appears to play an organizing role in the DMN (Fransson and Marrelec, 2008; Jiao et al., 2011). We therefore first nominated a mPC DMN "seed" vertex, empirically and without observer bias, using results of the largest existing meta-analytic delineation of the DMN (Laird et al., 2009), and then defined those cortical regions where rate of CT change was most highly correlated with that within the mPC seed. We hypothesized that correlations with mPC CT change would be maximal within mPFC and iPC DMN areas. We then further tested for elevated CT change correlations within the DMN using mPFC, iPC, and mPC seeds localized by an independent functional neuroimaging study (Fox et al., 2005). Finally, a second, "task positive" network (TPN) defined by this same independent study allowed us to asses if any observed maturational coupling changes were specific to the DMN, or also applied to other distributed cortical networks (Fox et al., 2005).

Our second test for convergence between the coordination of cortical development and cortical function focused on the relationship between CT changes at homologous cortical vertices. Functional coactivation of homologous points on the left and right cortical sheet is a core property of the healthy living brain (Toro et al., 2008), that exists in the context of dense interhemispheric white matter connectivity (Yorke and Caviness, 1975), and shows considerable stability across development (Zuo et al., 2010), and between species (White et al., 2011). Therefore, if structural connections and functional relationships within the cortical sheet are reflected in the way cortical regions develop with respect to one another, correlated CT change should be elevated in homologous, relative to nonhomologous pairings of contra-lateral vertices. To test this we statistically contrasted the distribution of all possible correlations between homologous vertices and the distribution of correlations between an equal number of nonhomologous left-right vertex pairings.

Finally, we asked if analysis of correlated CT change can reveal previously unidentified group differences in brain development by applying our methodology to test for sex differences in patterns of maturational coupling within the cortical sheet. Sex influences on maturational coupling are likely given that sex is known to modify several brain properties that could potentially reflect, or impact, the coordination of CT change, including cross-sectional patterns of CT correlation in the brain (Gong et al., 2009; Zielinski et al., 2010), and the ways in which different cortical regions are structurally (Menzler et al., 2011) and

functionally (Zuo et al., 2010) connected to each other. Consideration of sex-influences on brain development is especially pertinent within the developmental phase covered by our study. During adolescence prefrontal systems crucial for cognitive control (Christakou et al., 2009) undergo dramatic structural remodeling (Shaw et al., 2008), at the same time that well-documented sex differences emerge in markers of risk-taking behavior (e.g., accidental injuries) (Lyons et al., 1999; McQuillan and Campbell, 2006), road traffic accidents (Massie et al., 1995), and criminal offenses (Home Office, 2001) become disproportionately more common in males than females. Consequently, delineating sex effects on prefrontal maturation in adolescence may help to identify candidate neurodevelopmental mechanisms contributing to sex differences in cognition and behavior. This notion is supported by the findings of a recently published study, in which we carried out the first spatially fine-grained longitudinal map of sex differences in adolescent cortical development (Raznahan et al., 2010). By estimating group-average trajectories of CT change in males and females, we found evidence for delayed prefrontal cortical maturation in males relative to females. This delay was maximal in dorsolateral and ventrolateral prefrontal cortices (DLPFC and VLPFC, respectively), and associated with a left frontopolar cortex (FPC) focus of highly significant sex differences in the rate of adolescent cortical thinning (faster loss in males than females). These findings are relevant to our understanding of sex differences in adolescent behavior because the FPC, DLPFC, and VLPFC, are engaged when complex decisions requiring the coordination of multiple cognitive tasks in open-ended and affect-laden scenarios are made (Badre and Wagner, 2004; Pochon et al., 2002; Ramnani and Owen, 2004). In the current study therefore, we sought to build on our earlier work, by testing the hypothesis that—in addition to modifying the rate of left FPC CT change—sex also impacts the degree of maturational coupling between FPC and other prefrontal regions crucial for adaptive cognitive control and decision making such as the DLPFC and VLPFC.

RESULTS

Participant characteristics are detailed in Table 1.

Table 2 summarizes techniques used for data analysis and presentation of results in each of the following subsections.

Mapping Structural Change at the Group Level
The average rate of annual CT change at each vertex across all 108 participants is mapped in Figure 1. Using group-level estimates of CT change at each vertex, these maps replicate those derived by applying traditional mixed-model techniques to the same data set (see Figure S1 available online)—and thus establish that transformation of repeat intraindividual CT measures into person-specific maps of annualized CT change preserves group-level features of cortical maturation.

Regional Differences in Coordinated Cortical Maturation
To quantify how tightly coupled anatomical change at each vertex was with that throughout the rest of the cortical sheet,

Table 1. Participant Characteristics

Characteristic	Group			Sex Difference
	All	Male	Female	
Number of Individuals	108	67	41	n.s.
Singleton	63	35	28	
Member of twin pair	45	32	13	
Handedness, No.				n.s.
Right	99	62	37	
Mixed	4	3	1	
Left	5	2	3	
Race, No.				n.s.
Caucasian	98	62	36	
African-American	3	1	2	
Asian	2	1	1	
Hispanic	3	2	1	
Other	2	1	1	
IQ				n.s.
Mean (SD)	115 (11.8)	116 (11.5)	114 (12.4)	
SES				n.s.
Mean (SD)	40 (17.6)	39 (18.5)	41 (16.2)	
Number of scans, No.				n.s.
3 scans	67	39	28	
4 scans	31	22	9	
5 scans	9	5	4	
6 scans	1	1	0	
Total	376	236	140	
Age Distribution of Scans (years)				
Mean (SD)	15.2 (3.5)	15.3 (3.5)	14.9 (3.5)	
Range	9.1–22.8	9.2–22.7	9.1–22.8	

n.s., not statistically significant at p < 0.05; SES, socioeconomic status.

we correlated CT change at each vertex with that at all other vertices, and summed these correlations. As previously demonstrated for cross-sectional correlations in CT (Lerch et al., 2006), the results of this computationally expensive approach (involving over 3 billion correlations and taking ~6 days to complete per cortical hemisphere—with results as shown in Figure S2B) are adequately approximated by the more computationally efficient and interpretable method of correlating CT change at each vertex with a single measure of mean CT change across all vertices (results shown in Figure S2A [unthresholded] and Figure 2A [thresholded]). Therefore, the main body of our paper presents vertex-maps of correlation with mean CT change (Figure 2A), and does so after application of a $r \geq 0.3$ threshold (which excludes weak effect sizes according to Cohen's classification [Cohen, 1992]), to facilitate comparison with the only existing vertex-based maps of cross-sectional CT correlations (Lerch et al., 2006; reproduced in Figure 2C). Regardless of whether the relationship between CT change at each vertex and all others was represented (1) as a correlation with a mean CT change (Figures 2A and S2A); (2) as the sum of correlations with all other vertices (Figure S2B); or (3) after CT change at all vertices has been expressed as a proportion of starting CT

Table 2. Summary of Methods Used for Data Analysis and Presentation of Results

Objective	Analytic Method	Presentation of Results
1. Mapping rates of CT change at the group level	Average individual estimates of CT change at each vertex	Figure 1
	Use mixed models on repeat measures to derive an estimate of mean CT change at each vertex	Figure S1
2. Mapping regional differences in the strength of maturational coupling	Correlate interindividual differences in CT change at each vertex with interindividual differences in mean CT change (derived by averaging CT change across all vertices within each individual) using Pearson's correlation coefficient	Figure 2A (thresholded at r ≥ 0.3)
		Figure S2A (unthresholded)
	Correlate interindividual differences in CT change at each vertex with that at all other vertices to derive a vector of ~80,000 Pearson correlation coefficients at each vertex	Figure 2B (the proportion of these 80,000 r values that are ≥0.3)
		Figure S2B (the sum and the average of these 80,000 r values at each vertex)
3. Mapping regional differences in the strength of maturational coupling after adjusting the rates CT change for absolute CT	Re-express individual maps of CT change as proportions of starting CT at each vertex. Then correlate interindividual differences in adjusted CT change at each vertex with interindividual differences in mean adjusted CT change (derived by averaging adjusted CT change across all vertices within each individual) using Pearson's correlation coefficient	Figure S2C (unthresholded)
4. Defining cortical regions where CT change is most strongly correlated with that at a mPC DMN "seed" vertex	Correlate interindividual differences in mPC change with those at every other vertex to derive one Pearson's correlation coefficient at each vertex. Then quantify the strength of each r value relative to all possible 3 billion r values between 80,0000 vertices in the cortex as follows: (1) generate a distribution of r values by randomly sampling 500,000 pairs of vertices within the cortex, and (2) at each vertex, take the r value for correlation with mPC CT change, and calculate its centile position within the distribution of 500,000 r values to derive a centile value at each vertex	Figure 3A (unthresholded)
		Figure 3B (thresholded at ≥90th centile)
5. Determining if strength of maturational coupling between homologous vertices is significantly greater than that between nonhomologous contralateral vertex pairings	Correlate interindividual differences in CT change at each vertex in one hemisphere with interindividual change in its contralateral homolog to derive a distribution of ~40,000 Pearson correlation coefficients. Randomly sample 40,000 contralateral vertex-vertex pairings to derive 40,000 Pearson correlation coefficients. Statistically compare the mean of these two distributions using Mann-Whitney U test	N/A
6. Determining if individual maps of change can recover left frontopolar sex differences in rate of CT change as previously defined using mixed-models	Use t tests at each vertex to test if the distribution of CT change values in males and females differs	Figure S4B (thresholded t-statistic map after application of FDR correction with q = 0.05)
7. Comparing how left frontopolar CT change is coordinated with that in other cortical areas in males and females	Use linear regression to model interindividual differences in CT change at each vertex as a function of interindividual differences in left frontopolar CT change, sex, and the interaction of these two terms	Figure 4A (thresholded t-statistic map after application of FDR correction with q = 0.05 for main effect of left frontopolar CT change masked for regions where this is significantly modified by sex)
		Figure 4B (thresholded t-statistic map after application of FDR correction with q = 0.05 for interaction between sex and left frontopolar CT change)

CT, cortical thickness; FDR, false discovery rate; DMN, default mode network; mPC, medial posterior cortex.
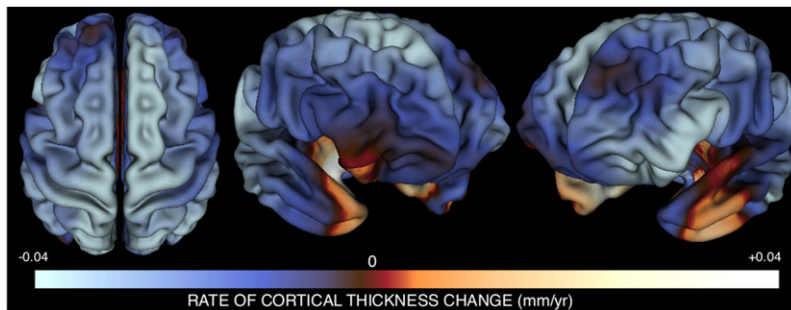
Figure 1. Mapping the Mean Rate of CT Change per Year between Ages 9 and 22 Years using Person-Specific Estimates of CT Change

Three views of the cortical sheet are shown. Colors represent the magnitude of mean annual cortical thickness (CT) change within our sample at each vertex. Mean change values were derived by averaging estimates of weighted annual CT change across all participants. Over the age range studied, most cortical regions are becoming thinner with advancing age, with the exception of bilateral anterior-medial temporal and right orbitofrontal cortices where CT is still increasing with age. This approach to mapping annual CT change closely replicates results derived using traditional mixed-model approaches for analyzing longitudinal data (Figure S1), and converges with other larger mixed-model studies of CT change (Shaw et al., 2008), but has the added advantage of permitting correlational analysis of interindividual differences in CT change at different vertices.

(Figure S2C)—correlations with global CT change were greatest in higher association cortices and least in primary sensory cortices. To convey this regional heterogeneity in more concrete terms, we mapped the proportion of the cortical sheet with which each vertex showed correlated CT change at or above a r ≥ 0.3 threshold (Figure 2B). This representation of the data again highlights fronto-temporal regions as showing the most spatially extensive maturational coupling with the remaining cortical sheet (covering up to 75% of the cortex), and primary sensory cortices as showing the least (covering less than 10% of the cortical sheet). Using the same 1% → 75% color scale shown in Figure 2B, these regional differences in the spatial extent of maturational coupling were visible across a wide range of r thresholds except those below 0.15 (i.e., almost all vertices are correlated with over 75% of the cortex at these low thresholds) or above 0.6 (i.e., very few vertices are correlated with greater than 1% of the cortex at these high thresholds) (see Figure S2D). Figures 2A and 2B also point toward asymmetries in CT change correlations, which we found to be statistically significant within inferior frontal, supramarginal and angular gyri (left > right), and in the ventral extent of the intraparietal sulcus (right > left).

In keeping with our hypothesis, regional differences in CT change correlations (Figure 2A) echoed previously published regional differences for correlations in cross-sectional measures of CT (reproduced in Figure 2C) (Lerch et al., 2006). Specifically, both maps show relatively strong correlations in perisylvian, lateral temporal, and medial frontal cortices, and relatively weak correlations in dorsal sensorimotor and occipital primary visual cortices. Apparent exceptions to this general picture of convergence include regions showing elevated correlations in CT, but not CT change (left lateral superior frontal and ventrolateral inferior frontal gyri), or visa-versa (ventromedial prefrontal cortex). To quantify concordance between maps of CT change correlation and cross-sectional CT correlation, we randomly selected a one-scan-per-person subset of our longitudinal data, and replicated the method used by Lerch et al. (2006) to derive correlation maps equivalent to those shown Figure 2C within our own sample. Intervertex differences in CT change correlation within our sample closely tracked intervertex differences in cross-sectional CT correlation (r = 0.79 correlation between maps). Similarity between correlation maps for CT and CT change could not have solely been a statistical artifact of any hidden relationship between CT change and cross-sectional CT, because it was not abolished by re-expressing estimates of annual CT change as a proportion of starting CT (i.e., Figure S2A is identical to Figure S2C).
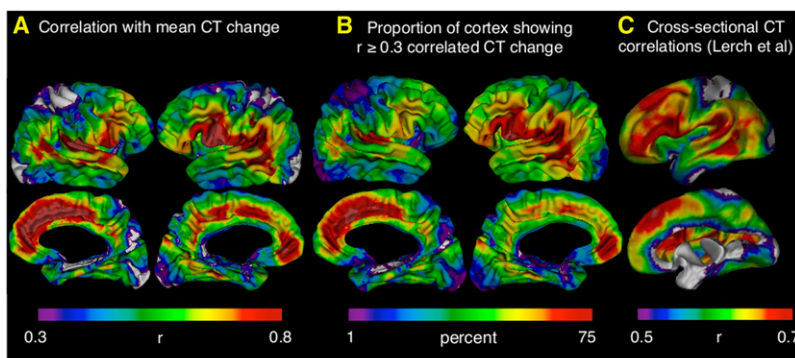

Figure 2. Regional Differences in Correlation with Rates of CT Change throughout the Cortical Sheet

(A) Map of correlation strength between CT change at each vertex and mean CT change across all vertices. This map has been arbitrarily thresholded at r ≥ 0.3 to highlight its similarity with a previously published thresholded map of cross-sectional CT correlations throughout the cortical sheet (Lerch et al., 2006). An unthresholded version of this map is provided in Figure S2A. Note that the strongest correlations with mean CT change are seen in fronto-temporal association cortices, whereas weakest correlations with mean CT change are seen in primary sensory cortices.

(B) An alternative representation of regional differences in maturational coupling. The color at a given cortical region represents the proportion of the cortical surface showing correlated CT change with the region in question at r ≥ 0.3. "Warmer" colors refer to higher proportions. Fronto-temporal regions show the most spatially extensive maturational coupling whereas primary sensory cortices show the least.

(C) A reproduction of earlier published (Lerch et al., 2006) maps showing the correlation between cross-sectional variation in CT at each vertex and mean CT across the whole vertex. Note the convergence between these maps and those for correlated CT change shown in (A) and (B).
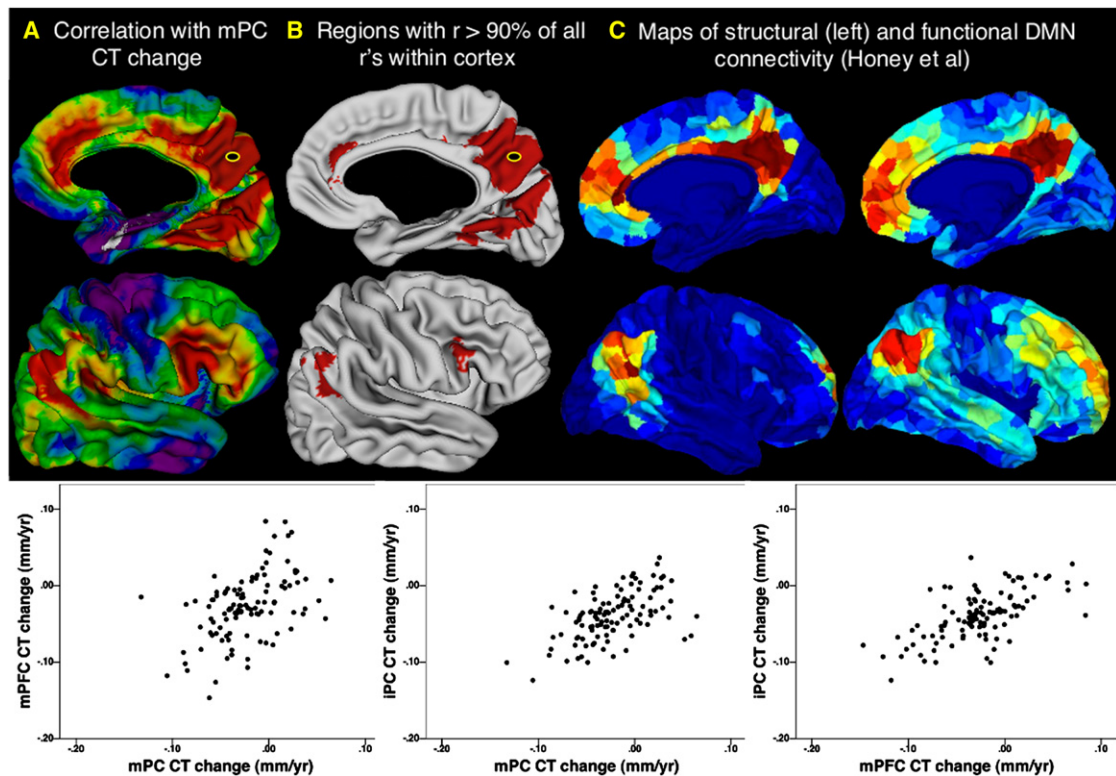
Figure 3. Maturational Coupling within the Default Mode Network

(A) Right hemisphere map of maturational coupling with the medial posterior cortex (mPC) default mode network (DMN) node. Color gradations represent correlation centile position in the distribution of all possible correlations between cortical vertices (blue → red: 1st → 100th centile).

(B) Regions where correlations with mPC change are in the top 90% of all possible correlations. Note mPFG and iPC overlaps between the distribution of regions showing highly coordinated maturation with the mPC DMN seed, and the distribution of regions that show high functional and structural connectivity within the DMN.

(C and D) Figures from Honey et al. (2009) depicting the DMN by analysis of diffusion tensor imaging and functional magnetic imaging resonance data, respectively.

Maturational Coupling Recapitulates Functional Coupling

To quantify the degree of maturational coupling within a well-established network of functionally and structurally interconnected cortical regions we first studied patterns of correlated CT change in the DMN. Rate of CT change within a bilateral mPC DMN seed selected through a meta-analysis of functional neuroimaging studies (Talairach coordinates: X, ±4; Y, −58; Z, +44) (Laird et al., 2009) was significantly correlated with that in widespread frontal, temporal and parietal cortices. However, the very strongest correlations with mPC change fell within one of the three predicted DMN centers: regions directly surrounding the mPC seed, mPFC, and iPL. This is illustrated for the right hemisphere in Figure 3. Figure 3A represents the CT change correlation between every vertex and the mPC seed as the centile position that correlation occupies in a distribution of 500,000 CT change correlations generated by randomly selecting pairs of vertices without regard to functional relatedness. Correlations in CT change between the mPC and other DMN centers are in the top 10% of all possible vertex-vertex CT change correlations in the cortical sheet (Figure 3B). Strong maturational coupling was also evident between the mPFC and iPL regions identified

using the mPC seed (inset plots, Figure 3). The relationship between anatomical maturation of the mPC and other DMN centers is not only strong, but also converges with several independent descriptions of cortical regions that structurally and functionally connected to mPC (Cauda et al., 2010; Fox et al., 2005; Greicius et al., 2003; Honey et al., 2009; Margulies et al., 2009; Uddin et al., 2009; van den Heuvel et al., 2008; Yu et al., 2011). To underline this, Figures 3C and 3D replicate illustrations from one such recently published study that sought to define those cortical regions showing maximal functional and structural (respectively) connectivity with the mPC (Honey et al., 2009). The only region in which we found strong and unpredicted correlations with mPC seed change was the bilateral inferior frontal gyrus (IFG). Interestingly, although not usually considered as part of the canonical DMN network, the IFG has shown strong functional and structural connectedness with the mPC in several studies of the DMN (Margulies et al., 2009; Uddin et al., 2009; Yu et al., 2011). There are however other inconsistently identified members of the DMN which we do not find to show strong maturational coupling with mPC, such as superior frontal and medial temporal cortices (Andrews-Hanna et al., 2010; Honey et al., 2009).

We next replicated our finding of elevated maturational coupling within the DMN using mPC, mPFC, and iPL nodes as independently defined in a previous resting-state functional MRI study (Fox et al., 2005), and used a "task positive network" (TPN) defined by this same study to establish that elevated maturational coupling is also a property of functionally-defined and spatially distributed brain networks other than the DMN. Mean CT change correlations within the DMN and TPN as defined by Fox et al. (2005) fell at the 91st and 88th centiles (respectively) of a random distribution of mean network CT change correlations generated by selecting 10,000 sets of 6-node networks, with each set consisting of three bilateral nodes, randomly selected without regard for functional relatedness.

Our analysis of correlated CT change between homologs provided further evidence for convergence between the coordination of cortical functioning and structural development. The modal correlation in CT change between homologous vertices was significantly higher than that between nonhomologous left-right vertex pairings ($p = 2.2 \times 10^{-16}$).

Analysis of Maturational Coupling Reveals Sex Differences in the Coordination of Prefrontal Cortical Maturation

We first established that our conversion of repeat CT measures to individual maps of annualized CT change was able to preserve group-level sex differences in left FPC CT change that we had previously identified using traditional mixed-model statistical within a larger longitudinal sample spanning the same age range (Raznahan et al., 2010; Figures S3A and S3B). We then statistically quantified sex differences in the extent to which interindividual differences in the rate of CT change within this left FPC seed (Talairach coordinates: X, −21; Y, 58; Z, −5) predicted those at every other vertex. The results of this analysis are summarized in Figure 4. Males and females showed strong and statistically indistinguishable positive relationships between the pace of left FPC CT change and that within widespread bilateral medial and lateral prefrontal, lateral temporal, angular and supramarginal, and superior parietal cortices (Figure 4A). Coupling with left FPC maturation was, however, significantly enhanced in females as compared to males in bilateral DLPFC and right VLPFC (Figure 4B). Enhanced coupling with left FPC maturation in males relative to females was restricted to small regions in the left orbitofrontal cortex, marginal sulcus, and parieto-occipital fissure. These findings held when analyses were conducted using CT change maps in which CT had been expressed as a proportion of starting CT (results not shown), suggesting that sex differences in maturational coupling are unlikely to be an artifact of differences in brain size between males and females.

DISCUSSION

The findings generated by our study of correlated anatomical change within the developing human brain fall into three broad groups.

First, we demonstrate that rates of anatomical change in different parts of the developing cortex show a highly
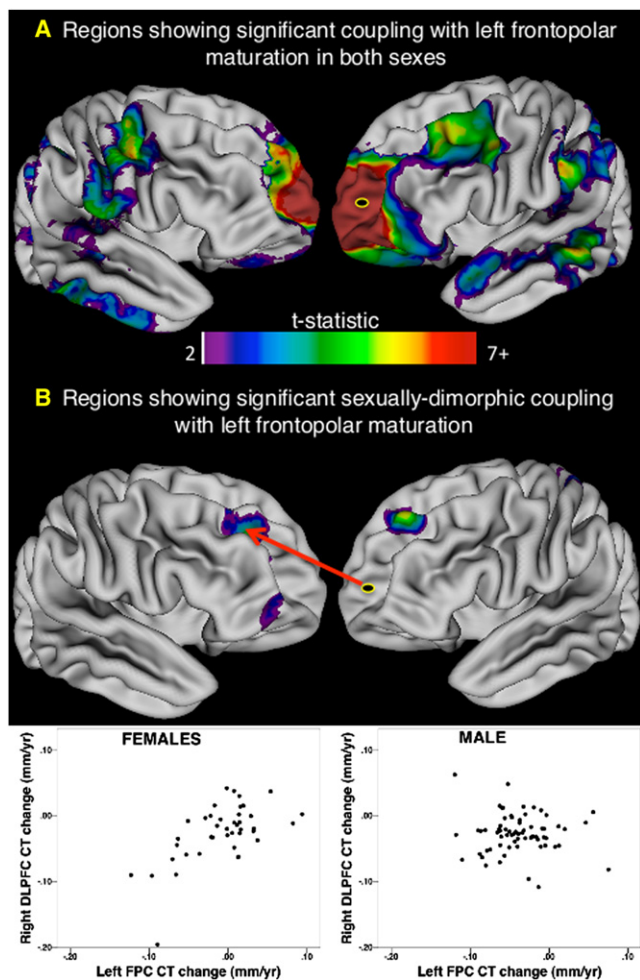

Figure 4. Maturational Coupling with the Left Frontopolar Cortex and Its Variation by Sex

The left frontopolar cortex (FPC) was used as a seed to explore sex differences in maturational coupling because it is where rate of cortical thickness (CT) change shows statistically significant sex differences over the age range studied—in both prior work (Raznahan et al., 2010; Figure S4A) and our current study (Figure S4B).

(A) Map of regions showing significant maturational coupling with left FPC that is not significantly different in magnitude between males and females. Note the very strong relationship between left FPC change and change at its contralateral homolog. Several regions show bilateral coupling with lFPC change (e.g., inferior temporal, planum temporale, angular gyrus and orbitofrontal cortex).

(B) Regions where coupling with lFPC CT change differs significantly between males and females. These consist of areas where coupling is specific to females, as shown for the right dorsolateral prefrontal cortex (rDLPFC) in the inset scatter plot. Furthermore, sex differences in FPC-DLPFC coupling also remained statistically significant after removal of nine outliers (defined using a conservative Cooks distance threshold of 4/n).

nonrandom correlational structure, and that the magnitude of this maturational coupling varies systematically across the cortical sheet. Specifically, rates of CT change in frontal and temporal association cortices display the strongest and most spatially extensive correlation with CT changes in the rest of

the cortex, whereas the opposite is seen in primary visual and sensorimotor cortices. These regional differences show several convergences with regional differences in cross-sectional CT correlation (Lerch et al., 2006), and we were able to rule out the possibility that these convergences solely arose as an artifact of hidden relationship between CT and CT change in our data set. A reasonable inference therefore is that patterns of cross-sectional CT correlation arise as a result of correlated maturation over time. By extension, established characteristics of cross-sectional CT correlation including its heritability (Schmitt et al., 2009), network modularity (Chen et al., 2008), and relationship with cognitive ability (Lerch et al., 2006) are likely to apply to correlated CT change, and these hypotheses can be directly tested in future work. The factors that might contribute to the regional differences in degree of coupling with global cortical maturation remain unclear. One possibility is that fronto-temporal cortices show more widespread maturational coupling than primary sensory cortices because they subserve more inte-grative cognitive processes that require functional coordination with greater swathes of the cortical sheet (Mesulam, 2000). An interesting observation in this regard is that within our predomi-nantly right-handed sample, cortical regions subserving left-lat-eralized language functions appear to be more closely coupled to the rest of the cortex than their contralateral counterparts, while the opposite is true for occipito-parietal regions linked to largely right-lateralized visuospatial functions.

Our second set of findings show that patterns of correlated CT change in development can be predicted from existing knowl-edge about the organizational architecture of cortical functioning and white-matter interconnectivity. In three different analyses, we find that correlations in CT change are unusually pronounced between cortical regions known to show strong interrelation-ships through prior functional neuroimaging studies of correlated brain activity (Greicius et al., 2003; Yu et al., 2011), diffusion tensor imaging of cortico-cortical white matter tracts (van den Heuvel et al., 2009), and postmortem tracer studies in primates (Burman et al., 2011). First, we were able to recover the core DMN as previously defined with diffusion tensor imaging and functional MRI (Buckner et al., 2008; Honey et al., 2009; van den Heuvel et al., 2009) by identifying those cortical regions where the rate of CT change is most tightly coupled with that within a mPC DMN seed selected through meta-analysis of functional neuroimaging data (Laird et al., 2009). We further established that the DMN shows elevated maturational coupling using independently generated coordinates for the mPF, mPFC, and iPC (Fox et al., 2005). Our additional finding of unusually strong CT change correlations within a second distributed functional network (the TPN) suggests that convergence between functional and maturational coupling may be a more general property of the brain. An important next step will be to delineate networks of coordinate maturation within the brain in an unbiased manner using graph-theory and related approaches (Bullmore and Sporns, 2009). An important aspect of this future work will be quantifying how patterns of maturational coupling within the brain change when varying correlational thresholds are applied. Second, our analysis of maturational coupling with the FPC recovered a network of cortical regions that closely replicates postmortem descriptions of FPC structural connec-tivity using tracer methods in the marmoset (Burman et al., 2011), and macaque (Petrides and Pandya, 1999) brain—en-compassing inferior temporal, orbitofrontal, and DLPFC regions. Reliance on primate data to infer white matter and functional connectivity of the FPC in humans is a difficulty however given known differences between humans and other primates in FPC anatomy (Ramnani and Owen, 2004). Third, we used random sampling methods to formally demonstrate that maturational coupling between pairs of homologous cortical regions is, on average, higher than that between pairs of nonhomologous vertices. A specific illustration of this general statement is provided by our analysis of maturational coupling with the left FPC; the cortical region showing most robust maturational coupling with the lFPC was the right FPC.

Taken together, our findings provide the first empirical support for an intimate relationship between the architecture of structural and functional cortical interconnectivity, and the way in which cortical regions structurally mature in relation to one another. This convergence adds a uniquely developmental perspective to a theme that is starting to emerge from multiple independent reports of similarity between descriptions of brain organization derived using different phenotypes. For example, parallels have now been drawn between patterns of brain organization defined by gene expression and structural connectivity (French and Pavlidis, 2011) as well as functional connectivity and white-matter connectedness (Honey et al., 2009). There is even some evidence that the coordination of anatomical changes in the brain over evolution is organized according to known patterns of structural connectivity between brain regions (Barton and Harvey, 2000). An important next step will be identifying the factors that underlie convergences (and divergences [Honey et al., 2009]) between different descriptions of brain organization. For example, does coordinated maturation within the DMN arise because members of the DMN are physically connected to, and function in concert with one another, and to what extent might the convergence between structural, functional and maturational coupling within the DMN be initiated by these regions sharing similar molecular profiles early on in cortical patterning? While the developmental experiments required to formally assess these causal models cannot be carried out in human popula-tions, several useful investigations of candidate mechanisms underlying our findings can be envisaged in humans. Twin studies could be used to measure the extent to which patterns of maturational and functional coupling within the brain reflect a common set of genetic influences (see Glahn et al. [2010] for a cross-sectional application of this approach to functional and structural connectedness within the DMN). Also, appropriately collected longitudinal data sets could be subjected to novel statistical methods that are currently being developed to examine causal hypotheses in human neuroimaging data (see Jiao et al. [2011] for an application of such methods to model causal relationships between activity in different DMN nodes). Understanding those causal mechanisms underlying the patterns of coordinated cortical maturation identified in this report will not only be relevant for models of typical brain devel-opment, but also shape thinking about the mechanisms under-lying neurodevelopment disease. For instance, if the coordina-tion of structural brain development is impacted by variations

in functional coupling (as has been demonstrated at the cellular level [Löwel and Singer, 1992]), then disorders with the potential to perturb functional connectivity in early life (Geschwind and Levitt, 2007) could disrupt patterns of coordinated brain maturation, and in doing so propagate over development to eventually manifest as distributed neuroanatomical abnormalities at later ages.

Our third set of findings relates to sex differences in the coordination of cortical maturation, and has two principal implications. First, by replicating our earlier report of sexually dimorphic CT change within the left FPC (Raznahan et al., 2010)—despite using a different methodology within a largely independent sample of scans—our data firmly establishes the FPC as key a region of interest for researchers seeking to delineate human brain systems that mature differently in males and females. Second, our findings stress the need to move beyond localization when seeking to understand how factors such as sex might impact brain development, and to explicitly model relationships between different brain regions. By modeling these relationships, we found that while female adolescents show a very close relationship between FPC and DLPFC maturation, male adolescents do not. The FPC and DLPFC are known to be structurally interconnected in nonhuman primates (Petrides and Pandya, 1999), and have been implicated in both flexible cognitive control and decision-making in humans (Badre and Wagner, 2004). Notably, FPC and DLPFC are most reliably engaged together by tasks that place high demands on working memory (Badre and Wagner, 2004) in open-ended, ill-defined, or reward-laden (Pochon et al., 2002) contexts and require the coordination of multiple higher cognitive processes for successful completion (Ramnani and Owen, 2004). We tentatively speculate therefore that sex differences in the tempo of adolescent FPC maturation and its coupling with DLPFC change may be relevant for developmental sex differences in the neural bases of cognitive control (Christakou et al., 2009), and the real-world sex differences in risk-taking and motivational control they may contribute to (Steinberg, 2010). There have been no published studies examining developmental influences on sex differences in FPC-DLPFC interactions during problem solving, and this will be an important area for future research, as will studies that directly test how sex and prefrontal maturational coupling interact to predict behavior. Our methodology for characterizing sex differences in maturational coupling could easily be extended to contrasts between disease groups and healthy controls.

The findings of our study should be considered in light of several caveats and limitations. First, CT development is known to follow a nonlinear trajectory from early childhood to early adulthood, but longitudinal neuroimaging data sets required to model these nonlinear trajectories within individuals are not yet available. Our correlational analysis of maturational coupling is therefore necessarily restricted to modeling age in a linear fashion at the individual level. This limits the generalizability of our findings beyond the age range studied, and assumes that patterns of maturational coupling do not change within the age range studied. It will be possible to directly assess the impact of this limitation, and explore the possibility to correlate nonlinear anatomical change across individuals once sufficient data exist.

Second, CT is only one of many morphological aspects of the cortical sheet, and correlated patterns of local anatomical change may differ for other aspects of cortical anatomy such as local surface area (as suggested by a recent report that cross-sectional correlation patterns for CT and surface area differ [Sanabria-Diaz et al., 2010]). Third, the cellular basis of CT change is not well understood, and need not necessarily reflect the same process in all cortical areas, or across different groups (e.g., males versus females). Therefore a correlation between the rate of CT change in two cortical regions does not necessarily imply that the same cellular process is occurring at the same rate in both of these areas. Similarly, two regions may show no correlation in overall CT change, while undergoing correlated changes in a given CT subcomponent (e.g., layer-specific changes). Fourth, we cannot comment on the processes that might underlie the correlations we study. Thus, correlations between the rate of CT change in two cortical regions (A and B) could be unidirectional (A → B or B → A), bidirectional (A ↔ B), or reflect the fact that CT change in both regions is tied to a common factor (e.g., the timing of developmental changes in gene expression, coordinated activity of these regions in the execution of different cognitive tasks) without their being any direct influence of change in one region upon that in the other.

Despite these limitations, our study represents the first ever investigation of correlated anatomical maturation in the developing human brain, and reveals that rates of structural cortical development in different cortical regions are highly organized with respect to one another and differ systematically in their magnitude between higher and lower-order cortices. Furthermore, cortical regions with strong structural and functional interconnectivity also show tightly coupled maturational tempos. Finally, over the adolescent age range covered by our study, rates of anatomical change, and their coordination with one another are sexually dimorphic within prefrontal subsystems crucial for self-regulation and cognitive control. The methods we present provide one way of moving longitudinal neuroimaging away from an exclusive focus on foci toward more integrative analyses that explicitly model how developmental changes in different brain regions are coordinated with one another.

EXPERIMENTAL PROCEDURES

Sample Characteristics and Image Acquisition

We included a total of 108 unrelated individuals (67 males/41 females) who had each had three or more sMRI scans at ~2-year intervals over the age range of 9–22 years. Participants were recruited through local advertisement. The absence of neurological or psychiatric illness was established through completion of a screening questionnaire (Childhood Behavior Checklist), and a structured diagnostic interview administered by a child psychiatrist (Giedd et al., 1999). Participants were of not selected for handedness (handedness established using Physical and Neurological Examination of Soft Signs). All participants had a full-scale intelligence quotient (FSIQ) greater than 80 (IQ was estimated using age-appropriate Wechsler Intelligence Scales [Shaw et al., 2006]). Socioeconomic status (SES) was quantified using Hollingshead scales (Hollingshead, 1975). Sample characteristics are detailed in Table 1.

All sMRI scans were T-1 weighted images with contiguous 1.5 mm axial slices and 2.0 mm coronal slices, obtained on the same 1.5-T General Electric (Milwaukee, WI) Signa scanner using a 3D spoiled gradient recalled echo sequence with the following parameters: echo time, 5 ms; repetition time,

24 ms; flip angle 45° (DEG); acquisition matrix, 256 × 192; number of excitations, 1; and field of view, 24 cm. Head placement was standardized as described previously.

The institutional review board of the National Institutes of Health approved the research protocol employed in this study and written informed consent and assent to participate in the study were obtained from parents/adult participants and children respectively.

Measuring Cortical Thickness

Native MRI scans were submitted to the CIVET pipeline (version 1.1.8) (http://wiki.bic.mni.mcgill.ca/index.php/CIVET) to generate separate cortical models for each hemisphere as described previously (Lerch and Evans, 2005). Briefly, this automated set of algorithms begins with linear transformation, correction of nonuniformity artifacts, and segmentation of each image into white matter, gray matter, and CSF (Zijdenbos et al., 2002). Next, each image is fitted with two deformable mesh models to extract the white/gray and pial surfaces. These surface representations are then used to calculate CT at ~40,000 vertices per hemisphere (MacDonald et al., 2000). A 30 mm bandwidth blurring kernel was applied, the size of which was selected to maximize statistical power while minimizing false positives—as determined by population simulation (Lerch and Evans, 2005). All cortical models were aligned through an automated surface-based registration algorithm (Robbins et al., 2004). The validity of these techniques for vertex-based estimates of CT are well-established (Shaw et al., 2008).

Creating Thickness Change Metrics

For each individual, repeat measures of CT at each vertex were used to derive a single estimate of mm CT change per year. This was done by dividing absolute total CT change at each vertex by the number of years over which repeat sMRI scans were available. This treatment of the data assumes linear CT change over the age range studied. Our correlational approach to defining patterns of maturational coupling within the cortex requires the presence of comparable person-specific estimates of anatomical change at multiple points throughout the cortex. Unfortunately, longitudinal studies of human brain development with scan densities necessary to confidently capture nonlinear changes in all cortical regions do not exist. This is because the developmental timing of curvilinear growth is known to vary widely across the cortical sheet (Shaw et al., 2008), and resolving curvilinear growth in all brain regions within an individual would therefore require an unfeasibly high rate of scans per year over an extended age range. In contrast, estimates of linear CT change can be generated from only two scans, and are known to be able to capture sex- (Raznahan et al., 2010), disease- (Vidal et al., 2006), and geno-type-related (Raznahan et al., 2010) differences in adolescent cortical maturation. We therefore restricted ourselves to modeling linear CT change with age within each person.

Statistical Analysis
Structural Change at the Group Level

Before using individual change maps to interrelate anatomical changes at different vertices, we tested if our conversion of repeat CT measures into person-specific maps of CT change was able to preserve group level characteristics of anatomical change as estimated using traditional mixed-model approaches. This was done by first using all person-specific change maps to calculate a group-average estimate of CT change at each vertex, and then comparing this group map for CT change to that for the β_1 coefficient in a mixed model, where, at each vertex, CT for ith individual's jth time-point was modeled as:

$$CT_{ij} = \text{Intercept} + d_i + \beta_1(\text{age}) + e_{ij}.$$

Structural Change Correlations across the Cortex

The statistical techniques used to correlate CT change at each vertex with that at all other vertices have been detailed in an earlier methodological paper, and are all based on Pearson's correlation coefficient (Lerch et al., 2006). In the current paper, we assessed the robustness of our maps for correlated CT change by deriving these maps in three different ways as outlined in Table 2, objectives 2 and 3.

Quantifying Asymmetry of CT Change Correlations

Correlations between CT change in left-hemisphere vertices and mean CT change overall were subtracted from equivalent correlations for right hemisphere homologs. Fisher's r to Z transformation was then used to determine if this left-right difference was significantly different from zero.

Correlated CT Change within the DMN and TPN

Our seed-based analysis of correlated CT change in the DMN involved: (1) specifying a mPC DMN seed in each hemisphere using peak coordinates provided by the largest existing functional neuroimaging DMN meta-analyses, and reflecting these about the midline (location in Talairach space: X, ±4; Y, −58; Z, +44); (2) correlating CT change at each mPC seed with CT change at all other ipsilateral vertices; and (3) assigning the resultant correlation coefficients a centile position within a distribution of 500,000 vertex-vertex correlations randomly sampled from the total distribution of all possible inter-vertex CT change correlations.

We also assayed CT change correlations within the DMN, using an independently defined set of mPC, mPFC, and iPL loci (Fox et al., 2005). This prior publication also provided loci for a second task positive network (involving bilateral intraparietal sulci, dorsolateral prefrontal cortex, and frontal eye fields), which we used to test for specificity of maturational changes to DMN.

Sex Differences in Correlation with Left FPC CT Change

We identified cortical regions where the mean rate of CT change differed between males and females using t tests at each vertex to compare mean rate of CT change between sex groups. The resultant map of t-statistics was thresholded using a false discovery rate (FDR) (Genovese et al., 2002) correction for multiple comparisons with q set at 0.05. This analysis identified a left FPC region where the mean rate of CT change in males was more negative than that in females. The rate of CT change at the peak vertex within this region (FPCδCT) was then used in a subsequent regression analysis where CT change (δCT) at each vertex was modeled as:

$$\delta CT_i = \text{Intercept} + \beta_1(\text{FPC}\delta CT) + \beta_2(\text{SEX}) + \beta3(\text{FPC}\delta CT \, {}^*\text{SEX}).$$

The t-statistics associated with the β_1 and β_3 coefficients were then mapped across the cortical sheet after thresholding with FDR correction (q = 0.05) to delineate (1) cortical regions in which rate of CT change was significantly predicted by that at FPC in a manner that did not differ significantly between males and females; and (2) regions where CT change showed a sexually dimorphic relationship with that at the FPC seed.

SUPPLEMENTAL INFORMATION

Supplemental Information includes four figures and can be found with this article online at doi:10.1016/j.neuron.2011.09.028.

REFERENCES

Andrews-Hanna, J.R., Reidler, J.S., Sepulcre, J., Poulin, R., and Buckner, R.L. (2010). Functional-anatomic fractionation of the brain's default network. Neuron 65, 550–562.

Badre, D., and Wagner, A.D. (2004). Selection, integration, and conflict monitoring; assessing the nature and generality of prefrontal cognitive control mechanisms. Neuron 41, 473–487.

Barton, R.A., and Harvey, P.H. (2000). Mosaic evolution of brain structure in mammals. Nature 405, 1055–1058.

Buckner, R.L., Andrews-Hanna, J.R., and Schacter, D.L. (2008). The brain's default network: anatomy, function, and relevance to disease. Ann. N Y Acad. Sci. 1124, 1–38.

Bullmore, E., and Sporns, O. (2009). Complex brain networks: graph theoretical analysis of structural and functional systems. Nat. Rev. Neurosci. 10, 186–198.

Burman, K.J., Reser, D.H., Yu, H.H., and Rosa, M.G. (2011). Cortical input to the frontal pole of the marmoset monkey. Cereb. Cortex 21, 1712–1737.

Cauda, F., Geminiani, G., D'Agata, F., Sacco, K., Duca, S., Bagshaw, A.P., and Cavanna, A.E. (2010). Functional connectivity of the posteromedial cortex. PLoS ONE 5, 5.

Chen, Z.J., He, Y., Rosa-Neto, P., Germann, J., and Evans, A.C. (2008). Revealing modular architecture of human brain structural networks by using cortical thickness from MRI. Cereb. Cortex 18, 2374–2381.

Christakou, A., Halari, R., Smith, A.B., Ifkovits, E., Brammer, M., and Rubia, K. (2009). Sex-dependent age modulation of frontostriatal and temporo-parietal activation during cognitive control. Neuroimage 48, 223–236.

Cohen, J. (1992). Quantitative methods in psychology: a power primer. Psychol. Bull. 112, 155–159.

Damoiseaux, J.S., Rombouts, S.A., Barkhof, F., Scheltens, P., Stam, C.J., Smith, S.M., and Beckmann, C.F. (2006). Consistent resting-state networks across healthy subjects. Proc. Natl. Acad. Sci. USA 103, 13848–13853.

de Bie, H.M., Boersma, M., Adriaanse, S., Veltman, D.J., Wink, A.M., Roosendaal, S.D., Barkhof, F., Stam, C.J., Oostrom, K.J., Delemarre-van de Waal, H.A., and Sanz-Arigita, E.J. (2011). Resting-state networks in awake five- to eight-year old children. Hum. Brain Mapp. Published online April 25, 2011. 10.1002/hbm.21280.

Draganski, B., Gaser, C., Busch, V., Schuierer, G., Bogdahn, U., and May, A. (2004). Neuroplasticity: changes in grey matter induced by training. Nature 427, 311–312.

Fair, D.A., Cohen, A.L., Dosenbach, N.U., Church, J.A., Miezin, F.M., Barch, D.M., Raichle, M.E., Petersen, S.E., and Schlaggar, B.L. (2008). The maturing architecture of the brain's default network. Proc. Natl. Acad. Sci. USA 105, 4028–4032.

Fox, M.D., Snyder, A.Z., Vincent, J.L., Corbetta, M., Van Essen, D.C., and Raichle, M.E. (2005). The human brain is intrinsically organized into dynamic, anticorrelated functional networks. Proc. Natl. Acad. Sci. USA 102, 9673–9678.

Fransson, P., and Marrelec, G. (2008). The precuneus/posterior cingulate cortex plays a pivotal role in the default mode network: Evidence from a partial correlation network analysis. Neuroimage 42, 1178–1184.

French, L., and Pavlidis, P. (2011). Relationships between gene expression and brain wiring in the adult rodent brain. PLoS Comput. Biol. 7, e1001049. 10.1371/journal.pcbi.1001049.

Gao, W., Zhu, H., Giovanello, K.S., Smith, J.K., Shen, D., Gilmore, J.H., and Lin, W. (2009). Evidence on the emergence of the brain's default network from 2-week-old to 2-year-old healthy pediatric subjects. Proc. Natl. Acad. Sci. USA 106, 6790–6795.

Genovese, C.R., Lazar, N.A., and Nichols, T. (2002). Thresholding of statistical maps in functional neuroimaging using the false discovery rate. Neuroimage 15, 870–878.

Geschwind, D.H., and Levitt, P. (2007). Autism spectrum disorders: developmental disconnection syndromes. Curr. Opin. Neurobiol. 17, 103–111.

Giedd, J.N., and Rapoport, J.L. (2010). Structural MRI of pediatric brain development: what have we learned and where are we going? Neuron 67, 728–734.

Giedd, J.N., Blumenthal, J., Jeffries, N.O., Castellanos, F.X., Liu, H., Zijdenbos, A., Paus, T., Evans, A.C., and Rapoport, J.L. (1999). Brain development during childhood and adolescence: a longitudinal MRI study. Nat. Neurosci. 2, 861–863.

Glahn, D.C., Winkler, A.M., Kochunov, P., Almasy, L., Duggirala, R., Carless, M.A., Curran, J.C., Olvera, R.L., Laird, A.R., Smith, S.M., et al. (2010). Genetic control over the resting brain. Proc. Natl. Acad. Sci. USA 107, 1223–1228.

Gogtay, N., Giedd, J.N., Lusk, L., Hayashi, K.M., Greenstein, D., Vaituzis, A.C., Nugent, T.F., 3rd, Herman, D.H., Clasen, L.S., Toga, A.W., et al. (2004). Dynamic mapping of human cortical development during childhood through early adulthood. Proc. Natl. Acad. Sci. USA 101, 8174–8179.

Gong, G., Rosa-Neto, P., Carbonell, F., Chen, Z.J., He, Y., and Evans, A.C. (2009). Age- and gender-related differences in the cortical anatomical network. J. Neurosci. 29, 15684–15693.

Gordon, C.T., Frazier, J.A., McKenna, K., Giedd, J., Zametkin, A., Zahn, T., Hommer, D., Hong, W., Kaysen, D., Albus, K.E., et al. (1994). Childhood-onset schizophrenia: an NIMH study in progress. Schizophr. Bull. 20, 697–712.

Greicius, M.D., Krasnow, B., Reiss, A.L., and Menon, V. (2003). Functional connectivity in the resting brain: a network analysis of the default mode hypothesis. Proc. Natl. Acad. Sci. USA 100, 253–258.

He, Y., Chen, Z.J., and Evans, A.C. (2007). Small-world anatomical networks in the human brain revealed by cortical thickness from MRI. Cereb. Cortex 17, 2407–2419.

Hill, J., Inder, T., Neil, J., Dierker, D., Harwell, J., and Van Essen, D. (2010). Similar patterns of cortical expansion during human development and evolution. Proc. Natl. Acad. Sci. USA 107, 13135–13140.

Hollingshead, A.B. (1975). Four-Factor Index for Social Status (New Haven: Yale UP).

Home Office. (2001). Criminal Statistics (Norwich, UK: Office of National Statistics).

Honey, C.J., Sporns, O., Cammoun, L., Gigandet, X., Thiran, J.P., Meuli, R., and Hagmann, P. (2009). Predicting human resting-state functional connectivity from structural connectivity. Proc. Natl. Acad. Sci. USA 106, 2035–2040.

Hyde, K.L., Lerch, J., Norton, A., Forgeard, M., Winner, E., Evans, A.C., and Schlaug, G. (2009). Musical training shapes structural brain development. J. Neurosci. 29, 3019–3025.

Jiao, Q., Lu, G., Zhang, Z., Zhong, Y., Wang, Z., Guo, Y., Li, K., Ding, M., and Liu, Y. (2011). Granger causal influence predicts BOLD activity levels in the default mode network. Hum. Brain Mapp. 32, 154–161.

Jolles, D.D., van Buchem, M.A., Crone, E.A., and Rombouts, S.A. (2011). A comprehensive study of whole-brain functional connectivity in children and young adults. Cereb. Cortex 21, 385–391.

Kabani, N., Le Goualher, G., MacDonald, D., and Evans, A.C. (2001). Measurement of cortical thickness using an automated 3-D algorithm: a validation study. Neuroimage 13, 375–380.

Kim, J.S., Singh, V., Lee, J.K., Lerch, J., Ad-Dab'bagh, Y., MacDonald, D., Lee, J.M., Kim, S.I., and Evans, A.C. (2005). Automated 3-D extraction and evaluation of the inner and outer cortical surfaces using a Laplacian map and partial volume effect classification. Neuroimage 27, 210–221.

Laird, A.R., Eickhoff, S.B., Li, K., Robin, D.A., Glahn, D.C., and Fox, P.T. (2009). Investigating the functional heterogeneity of the default mode network using coordinate-based meta-analytic modeling. J. Neurosci. 29, 14496–14505.

Lerch, J.P., and Evans, A.C. (2005). Cortical thickness analysis examined through power analysis and a population simulation. Neuroimage 24, 163–173.

Lerch, J.P., Worsley, K., Shaw, W.P., Greenstein, D.K., Lenroot, R.K., Giedd, J., and Evans, A.C. (2006). Mapping anatomical correlations across cerebral cortex (MACACC) using cortical thickness from MRI. Neuroimage 31, 993–1003.

Löwel, S., and Singer, W. (1992). Selection of intrinsic horizontal connections in the visual cortex by correlated neuronal activity. Science 255, 209–212.

Lyons, R.A., Delahunty, A.M., Kraus, D., Heaven, M., McCabe, M., Allen, H., and Nash, P. (1999). Children's fractures: a population based study. Inj. Prev. 5, 129–132.

MacDonald, D., Kabani, N., Avis, D., and Evans, A.C. (2000). Automated 3-D extraction of inner and outer surfaces of cerebral cortex from MRI. Neuroimage 12, 340–356.

Margulies, D.S., Vincent, J.L., Kelly, C., Lohmann, G., Uddin, L.Q., Biswal, B.B., Villringer, A., Castellanos, F.X., Milham, M.P., and Petrides, M. (2009). Precuneus shares intrinsic functional architecture in humans and monkeys. Proc. Natl. Acad. Sci. USA 106, 20069–20074.

Massie, D.L., Campbell, K.L., and Williams, A.F. (1995). Traffic accident involvement rates by driver age and gender. Accid. Anal. Prev. 27, 73–87.

McQuillan, R., and Campbell, H. (2006). Gender differences in adolescent injury characteristics: a population-based study of hospital A&E data. Public Health 120, 732–741.

Menzler, K., Belke, M., Wehrmann, E., Krakow, K., Lengler, U., Jansen, A., Hamer, H.M., Oertel, W.H., Rosenow, F., and Knake, S. (2011). Men and women are different: diffusion tensor imaging reveals sexual dimorphism in the microstructure of the thalamus, corpus callosum and cingulum. Neuroimage 54, 2557–2562.

Mesulam, M. (2000). Principles of Behavioral and Cognitive Neurology, Second Edition (Oxford: Oxford University Press).

Paus, T., Keshavan, M., and Giedd, J.N. (2008). Why do many psychiatric disorders emerge during adolescence? Nat. Rev. Neurosci. 9, 947–957.

Petrides, M., and Pandya, D.N. (1999). Dorsolateral prefrontal cortex: comparative cytoarchitectonic analysis in the human and the macaque brain and corticocortical connection patterns. Eur. J. Neurosci. 11, 1011–1036.

Pochon, J.B., Levy, R., Fossati, P., Lehericy, S., Poline, J.B., Pillon, B., Le Bihan, D., and Dubois, B. (2002). The neural system that bridges reward and cognition in humans: an fMRI study. Proc. Natl. Acad. Sci. USA 99, 5669–5674.

Raichle, M.E., MacLeod, A.M., Snyder, A.Z., Powers, W.J., Gusnard, D.A., and Shulman, G.L. (2001). A default mode of brain function. Proc. Natl. Acad. Sci. USA 98, 676–682.

Ramnani, N., and Owen, A.M. (2004). Anterior prefrontal cortex: insights into function from anatomy and neuroimaging. Nat. Rev. Neurosci. 5, 184–194.

Raznahan, A., Shaw, P., Lalonde, F., Stockman, M., Wallace, G.L., Greenstein, D., Clasen, L., Gogtay, N., and Giedd, J.N. (2011). How does your cortex grow? J. Neurosci. 31, 7174–7177.

Raznahan, A., Lee, Y., Stidd, R., Long, R., Greenstein, D., Clasen, L., Addington, A., Gogtay, N., Rapoport, J.L., and Giedd, J.N. (2010). Longitudinally mapping the influence of sex and androgen signaling on the dynamics of human cortical maturation in adolescence. Proc. Natl. Acad. Sci. USA 107, 16988–16993.

Robbins, S., Evans, A.C., Collins, D.L., and Whitesides, S. (2004). Tuning and comparing spatial normalization methods. Med. Image Anal. 8, 311–323.

Sanabria-Diaz, G., Melie-García, L., Iturria-Medina, Y., Alemán-Gómez, Y., Hernández-González, G., Valdés-Urrutia, L., Galán, L., and Valdés-Sosa, P. (2010). Surface area and cortical thickness descriptors reveal different attributes of the structural human brain networks. Neuroimage 50, 1497–1510.

Schmitt, J.E., Lenroot, R.K., Ordaz, S.E., Wallace, G.L., Lerch, J.P., Evans, A.C., Prom, E.C., Kendler, K.S., Neale, M.C., and Giedd, J.N. (2009). Variance decomposition of MRI-based covariance maps using genetically informative samples and structural equation modeling. Neuroimage 47, 56–64.

Seeley, W.W., Crawford, R.K., Zhou, J., Miller, B.L., and Greicius, M.D. (2009). Neurodegenerative diseases target large-scale human brain networks. Neuron 62, 42–52.

Shaw, P., Greenstein, D., Lerch, J., Clasen, L., Lenroot, R., Gogtay, N., Evans, A., Rapoport, J., and Giedd, J. (2006). Intellectual ability and cortical development in children and adolescents. Nature 440, 676–679.

Shaw, P., Kabani, N.J., Lerch, J.P., Eckstrand, K., Lenroot, R., Gogtay, N., Greenstein, D., Clasen, L., Evans, A., Rapoport, J.L., et al. (2008). Neurodevelopmental trajectories of the human cerebral cortex. J. Neurosci. 28, 3586–3594.

Sowell, E.R., Thompson, P.M., Leonard, C.M., Welcome, S.E., Kan, E., and Toga, A.W. (2004). Longitudinal mapping of cortical thickness and brain growth in normal children. J. Neurosci. 24, 8223–8231.

Steinberg, L. (2010). A dual systems model of adolescent risk-taking. Dev. Psychobiol. 52, 216–224.

Supekar, K., Uddin, L.Q., Prater, K., Amin, H., Greicius, M.D., and Menon, V. (2010). Development of functional and structural connectivity within the default mode network in young children. Neuroimage 52, 290–301.

Thomason, M.E., Dennis, E.L., Joshi, A.A., Joshi, S.H., Dinov, I.D., Chang, C., Henry, M.L., Johnson, R.F., Thompson, P.M., Toga, A.W., et al. (2011). Resting-state fMRI can reliably map neural networks in children. Neuroimage 55, 165–175.

Toro, R., Fox, P.T., and Paus, T. (2008). Functional coactivation map of the human brain. Cereb. Cortex 18, 2553–2559.

Uddin, L.Q., Kelly, A.M., Biswal, B.B., Xavier Castellanos, F., and Milham, M.P. (2009). Functional connectivity of default mode network components: correlation, anticorrelation, and causality. Hum. Brain Mapp. 30, 625–637.

van den Heuvel, M., Mandl, R., Luijges, J., and Hulshoff Pol, H. (2008). Microstructural organization of the cingulum tract and the level of default mode functional connectivity. J. Neurosci. 28, 10844–10851.

van den Heuvel, M.P., Mandl, R.C., Kahn, R.S., and Hulshoff Pol, H.E. (2009). Functionally linked resting-state networks reflect the underlying structural connectivity architecture of the human brain. Hum. Brain Mapp. 30, 3127–3141.

Vidal, C.N., Rapoport, J.L., Hayashi, K.M., Geaga, J.A., Sui, Y., McLemore, L.E., Alaghband, Y., Giedd, J.N., Gochman, P., Blumenthal, J., et al. (2006). Dynamically spreading frontal and cingulate deficits mapped in adolescents with schizophrenia. Arch. Gen. Psychiatry 63, 25–34.

Vincent, J.L., Patel, G.H., Fox, M.D., Snyder, A.Z., Baker, J.T., Van Essen, D.C., Zempel, J.M., Snyder, L.H., Corbetta, M., and Raichle, M.E. (2007). Intrinsic functional architecture in the anaesthetized monkey brain. Nature 447, 83–86.

White, B.R., Bauer, A.Q., Snyder, A.Z., Schlaggar, B.L., Lee, J.M., and Culver, J.P. (2011). Imaging of functional connectivity in the mouse brain. PLoS ONE 6, e16322.

Yorke, C.H., Jr., and Caviness, V.S., Jr. (1975). Interhemispheric neocortical connections of the corpus callosum in the normal mouse: a study based on anterograde and retrograde methods. J. Comp. Neurol. 164, 233–245.

Yu, C., Zhou, Y., Liu, Y., Jiang, T., Dong, H., Zhang, Y., and Walter, M. (2011). Functional segregation of the human cingulate cortex is confirmed by functional connectivity based neuroanatomical parcellation. Neuroimage 54, 2571–2581.

Zielinski, B.A., Gennatas, E.D., Zhou, J., and Seeley, W.W. (2010). Network-level structural covariance in the developing brain. Proc. Natl. Acad. Sci. USA 107, 18191–18196.

Zijdenbos, A.P., Forghani, R., and Evans, A.C. (2002). Automatic "pipeline" analysis of 3-D MRI data for clinical trials: application to multiple sclerosis. IEEE Trans. Med. Imaging 21, 1280–1291.

Zuo, X.N., Kelly, C., Di Martino, A., Mennes, M., Margulies, D.S., Bangaru, S., Grzadzinski, R., Evans, A.C., Zang, Y.F., Castellanos, F.X., and Milham, M.P. (2010). Growing together and growing apart: regional and sex differences in the lifespan developmental trajectories of functional homotopy. J. Neurosci. 30, 15034–15043.